Coverage-Dependent Adsorption Mode of Water on $Fe_3O_4(001)$: Insights from First Principles Calculations

Narasimham Mulakaluri,[†,‡] Rossitza Pentcheva,*[,†] and Matthias Scheffler[‡]

Department of Earth and Environmental Sciences, University of Munich (LMU), Theresienstr. 41, 80333 Munich, Germany, and Fritz-Haber-Institut der Max-Planck-Gesellschaft (FHI), Faradayweg 4-6, D-14195 Berlin, Germany

Received: January 13, 2010; Revised Manuscript Received: May 4, 2010

Using density functional theory calculations together with an on-site Coulomb repulsion term (GGA+U), we investigate the adsorption of water on $Fe_3O_4(001)$. Starting from a single water molecule per $(\sqrt{2} \times \sqrt{2})R45°$ unit cell, we vary the concentration and configuration of water and hydroxyl groups. Isolated water molecules on the clean surface tend to dissociate heterolytically with an OH group adsorbed on top of an octahedral iron and a proton donated to a surface oxygen. Furthermore, oxygen defects are found to promote strongly water dissociation. The released protons bind to distant surface oxygen to minimize the repulsive interaction between the surface OH groups. At higher coverages, the interplay between adsorbate−adsorbate and adsorbate−substrate interactions and the formation of hydrogen bonds between the surface species result in a crossover to a mixed adsorption mode where every second molecule is dissociated. The energetic trends are related to the underlying electronic mechanisms.

1. Introduction

Water plays a crucial role in many oxide-catalyzed reactions in the field of geochemistry, environmental sciences, and heterogeneous catalysis. Water adsorption can alter the catalytic reactivity, redox potential, and adsorption capacity of the surface[1] by influencing the electronic properties and availability of surface reaction sites. A fundamental understanding of how water molecules interact with metal oxide surfaces is essential[1,2] in order to control the catalytic properties. Important questions include the mode of adsorption (e.g., molecular or dissociative), the interaction between adsorbates, and the formation of functional groups and hydrogen-bonded networks.

Magnetite (Fe_3O_4) has versatile technical applications in magnetic recording media, as a potential material for spintronics applications, and as a catalyst. Some examples for the catalytic activity are the binding and reduction of heavy metals in environmental processes[3,4] or the high-temperature water gas phase shift reaction.[5] Because these reactions take place in a humid environment or in aqueous solutions, it is important to understand how water interacts with the $Fe_3O_4(001)$ surface.

Magnetite has an inverse spinel structure with a stacking of A layers and B layers in the [001] direction. The former contain tetrahedral iron (Fe_A) and the latter oxygen and octahedral iron (Fe_B). Although both bulk truncations of the crystal are polar of type three according to the classification of Tasker,[6] density functional theory (DFT) calculations[7,8] have recently shown that a distorted B layer is stabilized on the $Fe_3O_4(001)$, which explains the experimentally observed $(\sqrt{2} \times \sqrt{2})R45°$ reconstruction. The presence of both cations and anions on an oxide surface is typically considered to promote water dissociation, because the cation sites act as strong Lewis acids, attracting the lone pairs of the water molecule, and the surface oxygen acts a Brønsted base site, attracting the protons of the water molecule. However, NiO(001) is an example for a surface with both cations and anions exposed where only molecular adsorption has been reported so far.[9]

Despite intensive research on the clean $Fe_3O_4(001)$ surface, there are only a few studies on its interaction with water. Kendelewicz et al.[10] measured oxygen 1s core level shifts from X-ray photoemission spectroscopy (XPS). For low water vapor pressures, these were interpreted in terms of dissociative adsorption activated by surface defects. Beyond water vapor pressures of 10^{-3} to 10^{-4} mbar, an extensive hydroxylation was observed. The onset pressure is similar to values reported for the $Fe_3O_4(111)$[10] and α-$Fe_2O_3(0001)$[11] surfaces. On the other hand, water-immersed surfaces showed smaller chemical shifts. A broad feature at 1.6 eV was attributed to hydroxyl groups at nonequivalent sites. Furthermore, no sign of formation of a surface oxyhydroxide was found in near-edge extended X-ray adsorption fine spectra (NEXAFS) of the Fe L edge. In thermal-programmed desorption (TPD) experiments[12] of epitaxially grown $Fe_3O_4(001)$ films on a MgO(001) substrate, three desorption peaks were detected at 320, 280, and 225 K. These were associated with different chemisorbed states, but the exact adsorbate configurations and their relative stability cannot be directly accessed from experiment.

On the theoretical side, the water adsorption on $Fe_3O_4(001)$ has been studied by molecular dynamics (MD)[13,14] with empirical potentials. These studies point at a dissociative adsorption. However, in ref 14, the surface is modeled by a termination with a 0.5 ML (monolayer) of tetrahedral iron (0.5 A layer), which, according to DFT calculations,[7] is energetically unfavorable. First-principles calculations have proven very useful to resolve the energetic stability and structural properties of different adsorbate geometries. In a combined density functional theory (DFT) and low-energy electron diffraction (LEED) study,[15] we have recently presented a surface phase diagram obtained within the framework of ab initio atomistic thermodynamics.[16] Although this investigation has focused exclusively

* To whom correspondence should be addressed. E-mail: Rossitza.Pentcheva@lrz.uni-muenchen.de.
† LMU.
‡ FHI.

10.1021/jp100344n
Published on Web 06/08/2010

TABLE 1: Interatomic Distances[a] in Å and Tilt Angles in Degrees between OH Group and the Surface, as well as the H-O-H Angle of the Adsorbed Water Molecule

	d_{Fe-O^W}	$d_{Fe-O^{OH}}$	d_{O-H}	$d_{O^{OH}\cdots H^W}$	$d_{O^S\cdots H^W}$	Θ_{H-O^W-H}	$\Theta_{Fe-O^{OH}-H}$
$1D_V$-3		2.26	0.98				105.3
1F-1	2.22		0.97		2.54	106.5	
1D-1		1.84	0.97				120.3
2M	2.06	1.97	0.97/1.11	1.37	2.93	108.7	116.0
4M	2.09	1.98	0.97/1.10	1.40	2.90	109.5	114.5

[a] $d_{O^{OH}\cdots H^W}$ is the hydrogen bond between the adsorbed water and OH group in the mixed adsorption.

on the most stable configurations for given oxygen and water pressures, here, we present a detailed DFT study of the initial adsorption of water on $Fe_3O_4(001)$. We have varied systematically the concentration of water molecules on the surface and identify different stable and metastable physi- and chemisorbed configurations (sections 3.1, 3.3, and 3.4). Furthermore, in section 3.2, we investigate the role of surface defects on the adsorption mode of water. To explain the energetic trends, we analyze the structural and electronic properties of the systems. Because Fe_3O_4 is a strongly correlated material, we have considered the influence of electronic correlations within the GGA+U approach and explore, in section 3.5, the origin of differences between the GGA and GGA+U results. Finally, in section 3.6, we discuss the overall trends of the adsorption energy as a function of coverage and compare the adsorption properties of $Fe_3O_4(001)$ to other metal oxide surfaces. The results are summarized in section 4.

2. Computational Details

Density functional theory calculations were performed using the FP-LAPW (full potential linear augmented plane-wave) method in the WIEN2k[17] implementation. The generalized gradient approximation (GGA)[18] of the exchange-correlation potential is used. We have considered the influence of electronic correlations within the LDA/GGA+U[19] method applying U = 5 eV and J = 1 eV, similar to values used for bulk Fe_3O_4.[20,21] The muffin-tin (MT) radii are R_{Fe}^{MT} = 1.90 Bohr, R_O^{MT} = 1.10 Bohr, and R_H^{MT} = 0.60 Bohr. A mixed augmented plane-wave (APW+lo) and linear augmented plane-wave (LAPW) basis sets was used. Inside the MTs, the wave functions are expanded in spherical harmonics up to l_{max}^{wf} = 10. Nonspherical contributions to the electron density as well as potential are considered up to l_{max}^{pot} = 6. The energy cutoff for the plane-wave representation and potential are E_{max}^{wf} = 25 Ry and E_{max}^{pot} = 196 Ry, respectively. For the integration in the Brillouin zone, 16 $k_{||}$-points were used. Gas-phase O_2 and H_2O molecules are calculated in a box of 8 × 8 × 8 Å using the same cutoff parameters as for the slab calculation.[23]

The $Fe_3O_4(001)$ surface is modeled in the supercell geometry with slabs containing seven B layers and six A layers. Laterally, a $(\sqrt{2} \times \sqrt{2})R45°$ unit cell is used. Water is adsorbed on both sides of the inversion symmetric slab. The slab is separated in the z direction by a 12 Å vacuum from its periodic images to avoid spurious interaction. The lateral lattice constant of the supercell is set to the GGA bulk lattice constant of 8.41 Å, which is close to the experimental value of 8.39 Å. We have done full structural optimization of the various adsorbate configurations where the adsorbates along with the outer two AB layers are allowed to relax, whereas the central three AB layers are frozen to the bulk positions of the ions.

The systems contain typically 100−130 atoms, which results in a high numerical demand with matrix sizes for the diagonalization of up to 31 000 × 31 000. To reduce the computational cost and to search more efficiently for the most favorable adsorbate geometries, we have performed for some of the systems a structural optimization using the Vienna ab initio Simulation Package (VASP)[24] with a default cut-off energy for the plane-wave basis and a force relaxation up to 0.01 eV/Å. Using these geometries, several further relaxation steps were done subsequently with the WIEN2k code.

3. Results and Discussion

As mentioned above, DFT calculations predict that the clean $Fe_3O_4(001)$ surface is terminated by a modified B layer.[7,8] This result is supported by quantitative X-ray diffraction[7] and LEED[25] analyses and scanning tunneling microscopy measurements.[26] Starting from this termination,[27] we adsorb water molecules in different configurations. As there are four cationic sites per $(\sqrt{2} \times \sqrt{2})R45°$ unit cell, we have varied the coverage of water molecules from one to four (full saturation). Additionally, we have studied the adsorption of water molecules on a defective surface with one oxygen vacancy per $(\sqrt{2} \times \sqrt{2})R45°$ unit cell, which is stabilized at low oxygen pressures.[15]

In the following, we describe the adsorbate geometries, structural details, and relative stabilities of different configurations beginning with a single water molecule and successively increasing the coverage. The adsorption energy E_{ads} of H_2O to the $Fe_3O_4(001)$ surface in (eV/molecule) is described as

$$E_{ads} = \frac{1}{n}(E_{nH_2O:Fe_3O_4(001)} - E_{Fe_3O_4(001)} - nE_{H_2O}) \quad (1)$$

where n is the number of water molecules adsorbed. $E_{nH_2O:Fe_3O_4(001)}$ and $E_{Fe_3O_4(001)}$ are the total energies of the system with adsorbates and the clean surface, and E_{H_2O} is the energy of a gas-phase molecule. Structural parameters and adsorption energies are listed in Tables 1 and 2. To analyze the underlying mechanisms, the bonding character is discussed based on the electron density redistribution ($\Delta\rho$), which is defined as

$$\Delta\rho = \rho_{nH_2O:Fe_3O_4(001)} - \rho_{Fe_3O_4(001)} - \rho_{nH_2O} \quad (2)$$

where $\rho_{H_2O:Fe_3O_4(001)}$, $\rho_{Fe_3O_4(001)}$, and ρ_{nH_2O} are the electron densities of the system with adsorbates, the clean $Fe_3O_4(001)$ surface, and water molecules, respectively. In the reference systems, the positions of the atoms correspond to the ones in the adsorbate system.

3.1. Adsorption of an Isolated Water Molecule on the Nondefective $Fe_3O_4(001)$ Surface. We start the discussion with a single H_2O molecule on $Fe_3O_4(001)$ per $(\sqrt{2} \times \sqrt{2})R45°$ unit cell. The adsorbate geometries are shown in Figure 1. These include a molecular adsorption in an upright (1U) and flat (1F) geometry on top of surface octahedral iron (Fe_BS) as well as

TABLE 2: Adsorption Energies (eV/molecule) of Water Molecules Adsorbed in Different Configurations on Fe_3O_4(001) Obtained within GGA and GGA+*U*

	molecular, upright		molecular, flat		dissociative		mixed	
	GGA	GGA+*U*	GGA	GGA+*U*	GGA	GGA+*U*	GGA	GGA+*U*
1 H_2O	−0.62	−0.02	−0.70	−0.39	−0.66	−0.76		
2 H_2O	−0.30	−0.16	−0.45	−0.47	−0.34	−0.58	−0.80	−0.94
4 H_2O	−0.01	−0.02	−0.41	−0.51	−0.19	−0.43	−0.61	−0.82

dissociative adsorption where an OH group forms on top of Fe_BS and a proton goes either to a neighboring (1D-1) or to a distant surface oxygen (1D-2/1D-3). We find that 1U, where the hydrogen atoms point away from the surface (Figure 2a), has a nearly vanishing binding energy to the surface. The most favorable molecular configuration is 1F (−0.39 eV), where the molecule is nearly parallel to the surface with hydrogen atoms oriented toward surface oxygens (O^S) (1F, side view Figure 2b). However, the dissociative adsorption with a proton adsorbed either at a neighboring O^S (1D-1) (−0.73 eV) or at a more distant surface oxygen (1D-3) (−0.76 eV) turns out to be the most favorable configuration. In fact, all dissociated configurations have a similar adsorption energy, which is ∼0.3 eV lower than the value for molecular adsorption. Thus, the mode of adsorption for an isolated water molecule is dissociative, as reported also for Fe_3O_4(111).[28]

To shed more light on the adsorbate mode, we have investigated the electron density redistribution upon adsorption for the different adsorbate configurations. The $\Delta\rho$ and density of states (DOS) plots for an upright and flat H_2O molecule are shown in Figure 2. Molecular water adsorbs with oxygen pointing toward a surface Fe_B, and the main charge rearrangement takes place along the O^w-Fe_B bond. Only in the case of flat adsorption, there is some contribution of the neighboring surface oxygen that is involved in the formation of a hydrogen bond. We find a stronger accumulation of electron density between the molecule and the surface for the flat geometry, consistent with the stronger binding energy. Charge accumulation in the d_{z^2} orbital of Fe_BS on the side of the adsorbate indicates that it is the main orbital participating in the bonding. The pattern of electron rearrangement is consistent with the common understanding[2] that the adsorbate−surface interaction proceeds through a donation from the water lone pairs that act as a Lewis base into available Lewis acid surface orbitals of Fe_B.

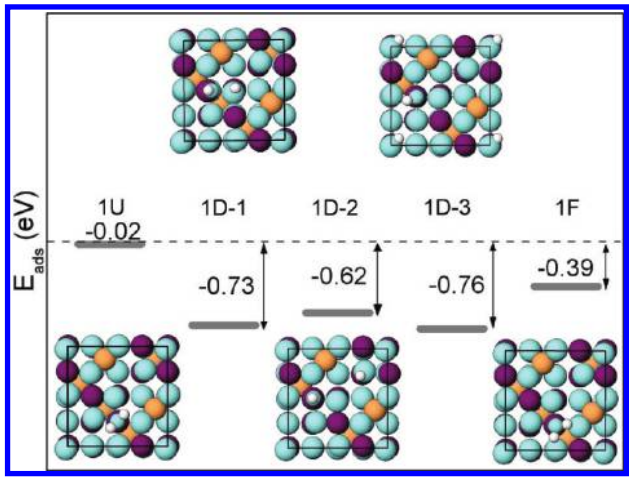

Figure 1. Top views of different adsorbate geometries of a single water molecule per $(\sqrt{2} \times \sqrt{2})R45°$ unit cell. The diagram shows the corresponding adsorption energies (in eV per molecule) obtained within GGA+*U*. Positions of oxygen, Fe_B, Fe_A, and H are marked by cyan, purple, orange, and white circles. The oxygens of the adsorbate are marked by smaller circles.

The main effects expected due to the interaction with the substrate are a shift of position and change in width of the molecular levels of the adsorbate.[29,30] Analysis of the partial DOS shows that, for the upright geometry, the $3a_1$ and $1b_1$ molecular levels (MO) of water remain very narrow. While $3a_1$ shifts by 1.5 eV to lower energies, the $1b_1$ state stays at the position of the gas-phase molecule. A narrow split-off d_{z^2} orbital of the lower Hubbard Fe 3d band overlaps with the $3a_1$ state. The weak interaction between occupied adsorbate orbitals and the substrate 3d band explains the vanishing E_{ads}.

For the flat/tilted adsorption, both the $3a_1$ and the $1b_1$ MO participate in the bonding to the surface. The stronger broadening/splitting observed here compared with the upright geometry indicates a stronger hybridization with the surface and a reduction of lifetime of the molecular states and is consistent with the higher E_{ads}. This electron redistribution serves to reduce Pauli's repulsion and to stabilize the system.[32] The electron density accumulation between molecule and substrate goes hand in hand with a depletion at the hydrogen positions, indicating a

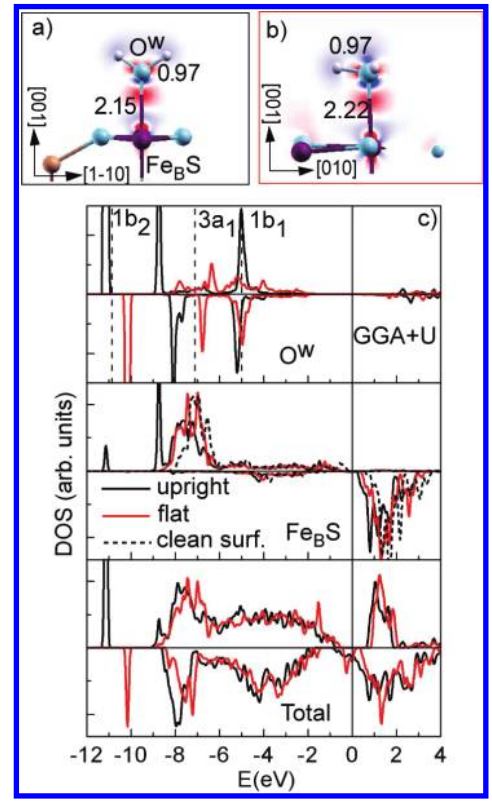

Figure 2. Electron density redistribution in a plane perpendicular to the surface obtained upon adsorption of a single water molecule in an (a) upright and (b) flat geometry. Electron density accumulation (depletion) is shown in red (blue). Positions of oxygen, Fe_B, and hydrogen are marked by cyan, purple, and white circles. (c) Total and projected density of states (DOS) at the oxygen and Fe_B sites for the two adsorbate geometries. The molecular orbitals of a gas-phase H_2O molecule are indicated by vertical dotted lines. These are obtained by aligning the $2a_1$ core level of the gas-phase and adsorbed H_2O molecule. The Fe 3d band of the clean surface is also shown with a dashed line.

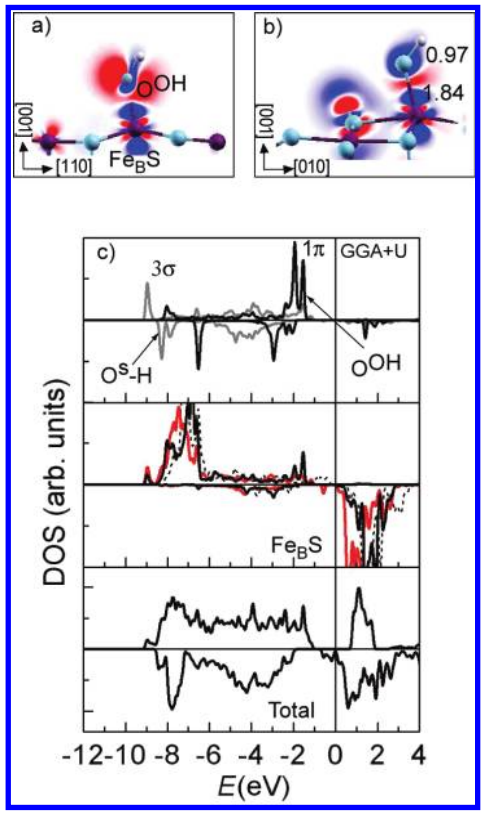

Figure 3. Electron density difference plots and DOS for the dissociative adsorption (1D-1) of an isolated H_2O molecule. $\Delta\rho$ is shown in a plane perpendicular to the surface along the (a) [110] and (b) [010] directions. The cut in (b) contains both the OH groups on top of a surface Fe_B and the protonated neighboring O^S. (c) Total and projected DOS (PDOS): (upper panel) PDOS of oxygen of the OH group on top of Fe_B (solid black line) as well as of the protonated neighboring surface oxygen (gray line); (central panel) PDOS of the 3d states of Fe_B with (solid black) and without (solid red line) an OH group on top. For comparison, the PDOS of Fe_B on the clean Fe_3O_4(001) surface is shown with a dashed line.

weakening of the OH bond. This is also expressed in a significant upward shift of the $1b_2$ molecular level of water in the case of 1F. The polarization of the OH bond goes hand in hand with a slight elongation of the bond from 0.96 Å for the gas-phase molecule to 0.97/0.98 Å for the upright/flat adsorbed molecule. In 1F, the hydrogen of the water molecule forms a hydrogen bond to a surface oxygen with a bond length of 2.54 Å. As a result of the interaction with the surface, the angle Θ_{H-O^w-H} is enhanced (106.5°). We have also optimized the tilt angle of the molecule w.r.t. the surface $\Theta_{Fe_B-O^w-H}$ and obtain ~102°. The large distance of the molecule to the surface Fe_B (1U, 2.15 Å; 1F, 2.22 Å) suggests a relatively weak overall interaction with the substrate. We note, however, that the bond lengths are shorter than the ones reported for molecular adsorption on 4d metal surfaces (2.3−2.7 Å).[31]

The strongest electron density redistribution is found for the dissociative adsorption (Figure 3a,b). We notice a significant charge transfer from Fe_BS d_{z^2} orbitals to the 1π MO of OH, which is now 1.5 eV below the Fermi level. Furthermore, there is a donation of charge from the 3σ lone pair of the OH ion to the t_{2g} states of the surface Lewis acid site. Conversely, charge is accumulated in the 3σ orbital of the OH group formed between a surface oxygen and the hydrogen of the dissociated H_2O (O^S-H). These features are further confirmed by the density of states in Figure 3c. The Fe_B 3d band is slightly broadened and shifted to lower energies w.r.t the one of the clean surface (dashed line). The lower Hubbard band, extending mainly between −8.5 and −6 eV, hybridizes predominantly with the 3σ molecular orbital of OH and only weakly with 1π. The splitting (lifting up of degeneracy) of the 1π MO strongly depends on the tilt angle $\Theta_{Fe_B-O^{OH}-H}$,[1] the optimum value of the latter being 120.3°. The strong electron redistribution for the dissociative adsorption invokes a pronounced outward relaxation of Fe_B and a shorter Fe_B-O^{OH} bond length of 1.84 Å compared with 2.15−2.22 Å for the molecular adsorption.

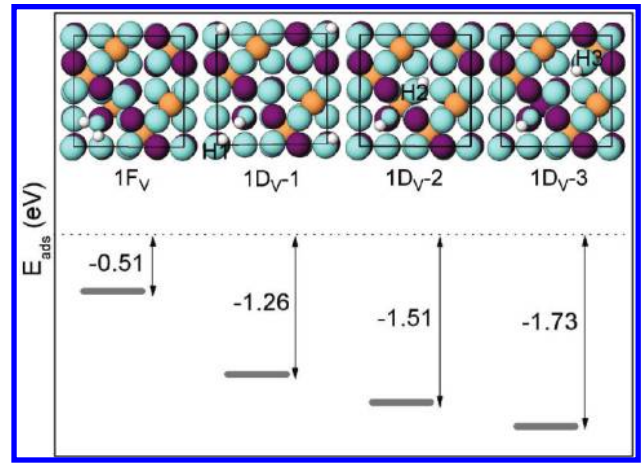

Figure 4. Schematic top views of different adsorbate geometries of a single water molecule adsorbed in an oxygen vacancy on the Fe_3O_4(001) surface. The solid gray lines show the adsorption energies (in eV per molecule) obtained within GGA+U.

Besides the heterolytic adsorption where an OH group is adsorbed on a cation site and a surface oxygen is protonated, we have also investigated a homolytic dissociation ($H_2O = HO + {}^1/_2H_2$), where ${}^1/_2H_2$ is released and a neutral HO is adsorbed on a cation site. This type of dissociation mechanism is highly endothermic (0.51 eV per H_2O molecule within GGA).

3.2. Adsorption of an Isolated Water Molecule on a Defective Fe_3O_4(001) Surface. Defects play an important role on oxide surfaces and can significantly influence the interaction of water with the surface. The relevant type of defects, especially at low oxygen pressures, are oxygen vacancies.[15] Here, we investigate the adsorption of water on a defective surface containing one oxygen vacancy (V_O) per $(\sqrt{2} \times \sqrt{2})R45°$ surface unit cell, which corresponds to a defect concentration of ~12.5%. The vacancies are separated by 8.41 Å from each other; thus, their interaction is negligible. The formation energy of one V_O per $(\sqrt{2} \times \sqrt{2})R45°$ unit cell is calculated as $E_f = E_{Fe_3O_4(001)-V_O} + {}^1/_2E_{O_2} - E_{Fe_3O_4(001)}$, where $E_{Fe_3O_4(001)-V_O}$ and $E_{Fe_3O_4(001)}$ are the total energies of the Fe_3O_4(001) surface with and without oxygen defects and E_{O_2} is the energy of a gas-phase oxygen molecule. We find that the formation energy is 1.08 eV higher for an oxygen vacancy with a neighboring Fe_A (3.51 eV) than without (2.47 eV). The latter type of oxygen vacancies is, therefore, expected to prevail and has been further considered for the adsorption of water.

Figure 4 shows the adsorption models studied on the defective surface along with the corresponding adsorption energies. Besides the molecular adsorption of H_2O in a vacancy, we have investigated a number of dissociative configurations where an OH group occupies the vacancy and a hydrogen is adsorbed at different surface oxygen sites (configurations $1D_V$-1, $1D_V$-2, and $1D_V$-3). The bonds between oxygen of the flat/tilted molecule and the neighboring Fe_B ($d_{O_w-Fe_BS} = 2.75$ Å, $d_{O_w-Fe_B(S-1)} = 2.63$ Å) are much longer than the O^w-Fe_BS distance on the nondefective surface (2.22 Å). Still, the adsorption energy is

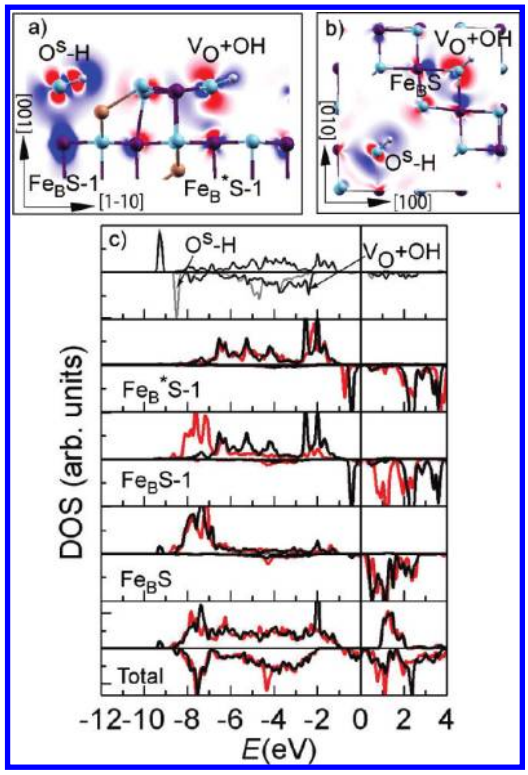

Figure 5. Electron density difference plots and DOS of a single water molecule dissociated in an oxygen vacancy on the $Fe_3O_4(001)$ surface ($1D_V$-3). (a, b) Cross sections of $\Delta\rho$ perpendicular and parallel to the surface, respectively. (c) (top panel) The projected DOS on the oxygen of the OH group in the vacancy and the protonated surface oxygen; (central panel) PDOS of the 3d states of a surface Fe_B next to the vacancy (Fe_BS), as well as the Fe_B ions beneath the vacancy (Fe_B^*S-1) and beneath O^S−H (Fe_BS-1) are shown. Black and red lines indicate the DOS before and after adsorption of the molecule, showing also a change in valence state at Fe_BS-1.

significant (−0.51 eV). This is related to the higher coordination of the molecule in the V_O than on the nondefective surface. Also, the much broader majority spin band at Fe^{2+} in the subsurface layer (not shown here but similar to Fe_B^*S-1 in Figure 5c) allows a stronger hybridization with the molecular orbitals of H_2O.

On the defective surface, the dissociative adsorption is strongly favored (by 0.75−1.23 eV) over the molecular. While on the defect-free surface, several proton binding sites have similar energies, here, the proton prefers a distant O^S (configuration $1D_V$-3). This indicates a repulsive interaction between the surface OH groups and results in a distribution of the OH groups at a distance of 5.95 Å. The O^S−H and OH tilt strongly toward the opposite O^S in order to form a hydrogen bond, thereby aligning themselves nearly parallel to the surface.

The electron density difference plots for the dissociative adsorption in a defect ($1D_V$-3) are displayed in Figure 5a,b. The hydroxyl group in the vacancy shows an accumulation in the 1π orbital and depletion in the 3σ orbital, whereas the 3σ orbital is occupied upon formation of the O^S−H group. We note that O^S−H in $1D_V$-3 (Figure 5c) has an even stronger splitting of the 1π orbital compared to that in 1D-1 (Figure 3c).

An interesting feature is that the OH group in the vacancy forms stronger bonds to the neighboring Fe_BS (stronger charge redistribution within the Fe_B 3d orbitals) than to the Fe_B underneath [Fe_B(S-1)]. This is expressed in an elongated Fe_B(S-1)−O^{OH} bond length of 2.26 Å. The dissociative adsorption in a vacancy induces significant electronic/valence changes

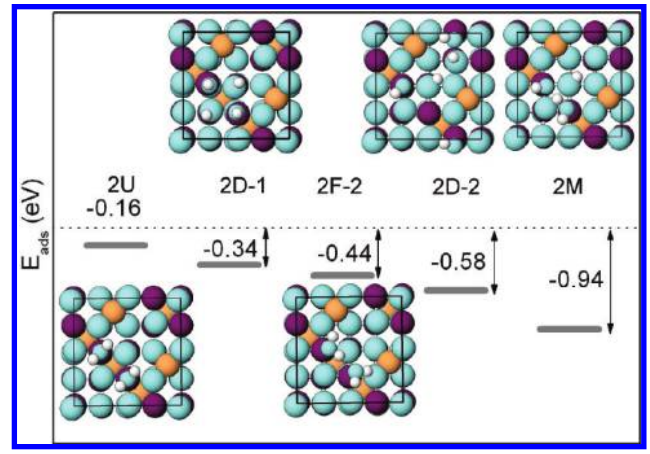

Figure 6. Top views of different adsorbate geometries of two water molecules per $(\sqrt{2} \times \sqrt{2})R45°$ unit cell. The diagram above shows the adsorption energies (in eV per molecule) obtained within GGA+U (solid gray lines). For the color coding, see Figure 1.

in the magnetite surface: At the defective surface, the two subsurface Fe_B around the vacancy are Fe^{2+}. Upon adsorption, both Fe_B(S-1) sites underneath the surface OH groups become Fe^{2+}. This effect of electron transfer may have important implications in understanding the catalytic activity of $Fe_3O_4(001)$. For a more detailed analysis of the charge ordering, the reader is referred to ref 15.

3.3. Adsorption of Two Water Molecules. With the inclusion of a second H_2O molecule, the adsorbate−adsorbate interaction sets in besides the adsorbate−substrate interaction. We have considered a variety of models of two adsorbed H_2O molecules and present in Figure 6 only the most stable ones. In the most favorable molecular configuration, 2F-2 (−0.44 eV), the two molecules are oriented parallel to the surface, one pointing with one of the OH bonds along the [110] direction acting as a proton donor and the other one acting as a proton acceptor. Additionally, the latter forms a hydrogen bond with a surface oxygen.

Furthermore, two dissociated configurations are displayed in Figure 6. The one with OH groups adsorbed on adjacent Fe_BS sites (2D-1) is 0.24 eV less favorable than 2D-2 where Fe_BS sites with and without adsorbed OH groups alternate. The latter geometry is preferred because it decreases the repulsive interaction between the OH groups on top of Fe_BS and facilitates hydrogen bond formation between O^S−H···O^S−H.

The most stable configuration turns out to be the one where partial dissociation of water takes place (2M) (E_{ads} = −0.94 eV). Here, one molecule dissociates and the hydrogen forms an OH group with a neighboring O^S. The intact molecule is oriented toward the OH group, forming a hydrogen bond. The proton at O^S shifts from the on-top position toward the opposite O^S, thereby also making a hydrogen bond.

Configuration 2F-2 can be considered as a precursor for the partial dissociation; therefore, we discuss in the following the structure of 2F-2 and 2M (shown in Figure 7a,b) in more detail. In 2F-2, one of the molecules, denoted H_2O-I, which is in a flat geometry, acts as a hydrogen-bond donor to the second H_2O and to the neighboring O^S, whereas H_2O-II is strongly tilted with one hydrogen oriented toward a neighboring surface oxygen and the second pointing away from the surface. The different adsorbate orientations with respect to the surface results in a difference of 0.12 Å in the Fe_B−O^w bond length. The water dimer distance is 1.86 Å, which is quite close to that observed for a gas-phase dimer (1.88 Å). The formation of a hydrogen

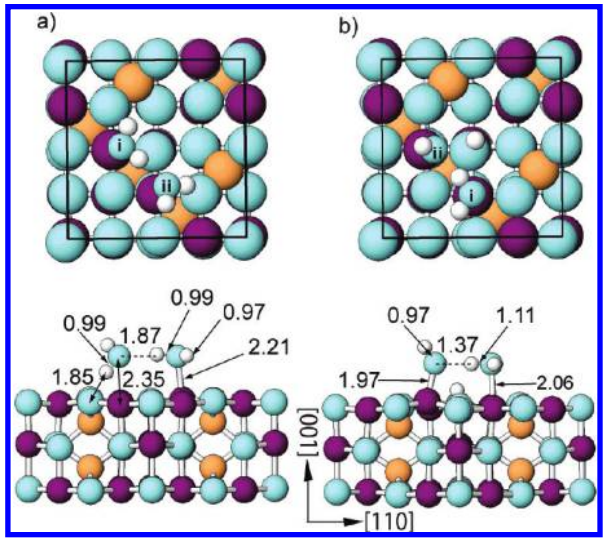

Figure 7. Top and side views of (a) two hydrogen-bonded water molecules (2F-2) and (b) a mixed molecular and dissociative adsorption (2M).

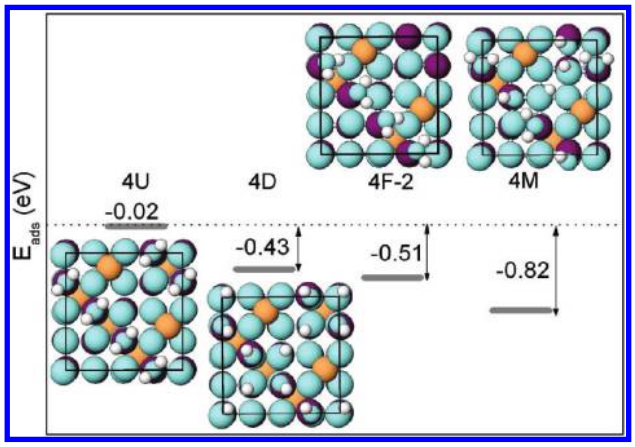

Figure 8. Top views of different adsorbate geometries of four water molecules adsorbed on Fe_3O_4(001). The diagram shows the adsorption energies (in eV per molecule) obtained within GGA+*U*. For the color coding, see Figure 1.

bond to O^S and between the two molecules leads to weakening of the OH bonds (bond length increased to 0.97−0.99 Å). This facilitates the dissociation of H_2O-II, resulting in configuration 2M.

Another possible scenario for the mixed adsorption is that, after an initial dissociation of isolated H_2O, further molecules arriving on the surface form hydrogen bonds with the present OH groups, resulting in the 2M configuration.

In the partially dissociated case (Figure 7b), the adsorbate−adsorbate (H_2O−OH) interaction results in a longer Fe_B−O^{OH} bond (1.97 Å) compared with the one of an isolated dissociated molecule (1.84 Å). On the other hand, the Fe_B−O^w bond length is 2.06 Å, significantly shorter than in the case of the isolated molecule (1F, 2.22 Å) and identical to the bulk Fe_B−O value. The stronger interaction between H_2O and OH in 2M is reflected in a 0.50 Å shorter $O^{OH}\cdots H^{H_2O}$ bond length (1.37 Å) in 2M compared with the $O^w\cdots H^{H_2O}$ distance in 2F-2 (1.87 Å).

3.4. Adsorption of Four Water Molecules. The adsorption of four H_2O molecules completely saturates the surface cationic sites. The different configurations are shown in Figure 8. The most favorable adsorption mode is again the mixed adsorption (4M) with an adsorption energy of −0.82 eV. Similar to the two-molecule case, this is followed in stability by a hydrogen-bonded chain (4F-2) (0.3 eV less favorable) of flat molecules where every second H_2O provides a hydrogen bond both to the neighbor (which itself is tilted) and to a surface oxygen. The dissociative adsorption is 0.4 eV less stable.

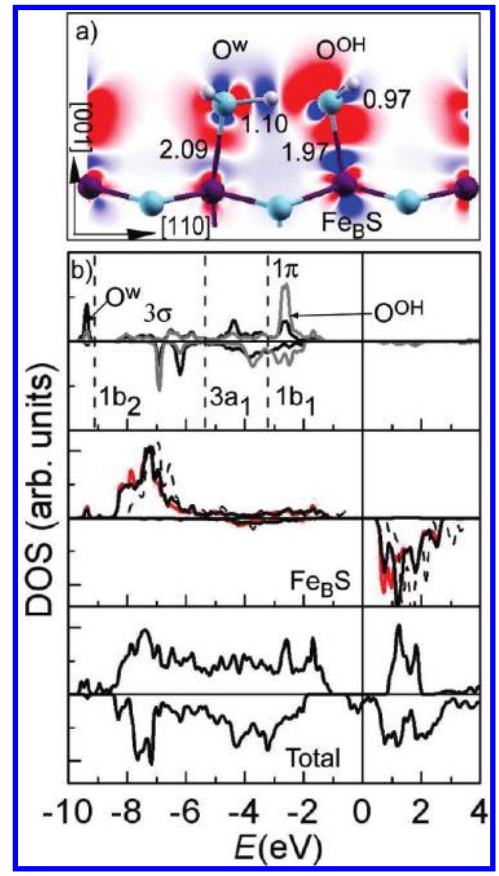

Figure 9. Four H_2O in a mixed adsorption mode (4M): (a) Difference density plot showing a cut perpendicular to the surface along the [110] direction and (b) (upper panel) PDOS of the O^w (black) and O^{OH} (gray). The molecular orbitals of a gas-phase H_2O molecule are indicated by vertical dotted lines. The central panel shows the 3d bands of Fe_B with an adsorbed H_2O molecule (black) and an OH group [red (gray)]. For comparison, the PDOS of Fe_B on the clean surface is displayed (black dashed line). The third panel shows the total DOS.

The electron density redistribution upon adsorption shown in Figure 9 bears some similarities to $\Delta\rho$ of the isolated flat (Figure 2) and dissociated (Figure 3) molecules. For example, the d_{z^2} orbital of Fe_B hybridizes with the MO of water. For the dissociated molecule, an accumulation of the 1π and depletion in the 3σ orbital of the OH group is observed, similar to the case of an isolated dissociated molecule (1D-1). We find also a pronounced outward relaxation of Fe_B toward the OH group, leading to an Fe_B−O^{OH} distance of 1.97 Å. Still, this bond is 0.13 Å longer than the one in the isolated dissociated molecule. On the other hand, Fe_B−O^w (2.09 Å) is 0.13 Å shorter than in the isolated flat molecule (1F). These differences are associated with the intermolecular interaction. An important feature is the predicted two distinct bond lengths Fe_B−O^w (2.09 Å) and Fe_B−O^{OH} (1.97 Å). This feature is supported by a quantitative LEED analysis.[15]

The formation of a hydrogen bond between the H_2O molecule and the neighboring OH group leads to a significantly elongated O^w−H distance of 1.10 Å. Furthermore, the O^{OH} exhibits a strong lateral shift from the on-top position toward the neighboring H_2O, which itself is strongly tilted as compared with the isolated molecule (Figure 2). The DOS in Figure 9 shows a much stronger broadening and splitting of the $3a_1$ and $1b_1$

states of H_2O compared with the isolated molecule case, indicating a stronger hybridization not only with the surface but also to the neighboring adsorbates. Likewise, the degeneracy of the 1π MO of OH is lifted and exhibits a bondng/antibonding splitting. It is interesting to note that the PDOS of O^{OH} and O^{w} are very similar, especially in the range between −6 and −8.5 eV, illustrating that hydrogen is shared between H_2O and the neighboring OH. The hybridization to the substrate is expressed by a shift of the occupied 3d band of Fe_BS to lower energies.

The difference between the total energy of a free-standing adsorbate layer and the total energies of isolated OH and H_2O gives an estimate of the contribution due to hydrogen bonding to E_{ads}. We note that systematic studies[34,35] have shown that the PBE[18] functional gives a good description of hydrogen bonding w.r.t. equilibrium geometries with error bars of ±0.02 eV. Both for 2M and 4M, we obtained ∼0.37 eV per molecule. This emphasizes the contribution of hydrogen bonding in stabilizing the partial dissociation on the $Fe_3O_4(001)$ surface.

3.5. Comparison between GGA and GGA+*U* Results. Already for the clean $Fe_3O_4(001)$ surface, the level of description of electronic correlations leads to significant qualitative differences in the electronic properties, albeit the energetic trends between different terminations are similar. Within GGA, states in the majority band gap lead to a metallic behavior at the surface.[7] In contrast, GGA+*U* correctly describes the opening of an insulating band gap,[8,15] as observed experimentally in scanning tunneling spectroscopy measurements.[37] In the case of water adsorption, we find that, especially for higher coverages, the trends within GGA and GGA+*U* are consistent (energy differences are within 0.2 eV; see Table 2).

However, there are some discrepancies in the case of an isolated molecule on the nondefective surface, which we would like to discuss in more detail in the following. Within GGA, the molecular adsorption where the water molecule is parallel to the surface with the hydrogen atoms pointing toward neighboring surface oxygens (1F) is found to be energetically most favorable (−0.70 eV), followed by the dissociative adsorption (−0.66 eV) and an adsorption in an upright position (1U) with the hydrogen atom pointing away from the surface (−0.62 eV). We note that, within GGA+*U*, the latter had a vanishing binding energy.

In contrast to transition-metal surfaces,[31,33] where the Fermi level crosses the d band, here, both the adsorbate orbitals and the substrate majority 3d band are occupied. Therefore, the interaction is not expressed by a change of occupation of levels but mainly by broadening of molecular orbitals. The main feature that is observed within GGA for the upright adsorption (cf. Figure 10) is a significant broadening of the $1b_1$ state. As the latter is closest to the Fermi level, it has a dominating influence on the stability. The hybridization with the broad Fe_B 3d band, which extends from −7 eV to the Fermi level, reduces the Pauli repulsion[32] and stabilizes the molecular adsorption in an upright geometry within GGA. In contrast, within GGA+*U*, the $1b_1$ level remains very narrow due to the lack of overlap with the narrow Fe 3d band whose main peak lies between −8 and −6 eV, thus favoring hybridization mainly with the $3a_1$ state of the adsorbate.

A further issue concerns the adsorption of water on a defective surface: Although both GGA and GGA+*U* predict dissociation, the corresponding energies are 0.98 and 1.73 eV, respectively. The difference of 0.75 eV is ascribed to the different formation energies of a vacancy on the $Fe_3O_4(001)$ surface: 1.67 eV (GGA) and 2.47 eV (GGA+*U*). This is related to the different degrees of localization of the electronic charge around the V_O and the resulting structural relaxation. We note that an even larger variation of 1.5 eV between GGA and GGA+*U* was found for $TiO_2(110)$.[36]

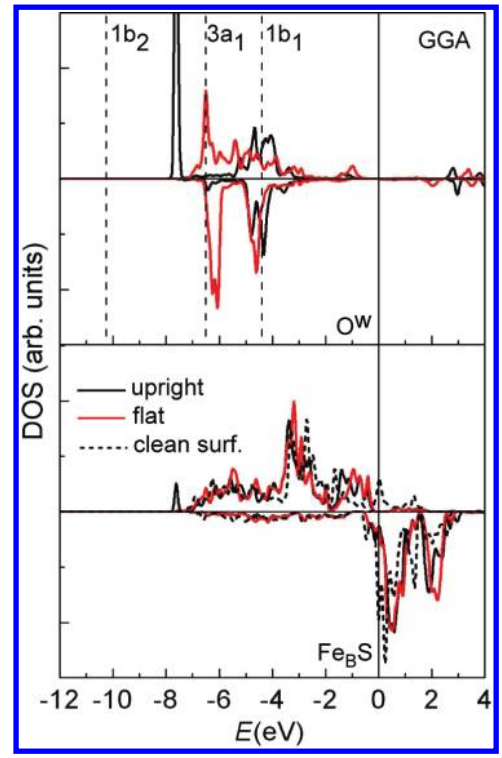

Figure 10. Total and projected DOS of 1U and 1F configurations obtained with GGA. The corresponsing results within GGA+*U* are shown in Figure 2. The molecular orbitals of a gas-phase H_2O molecule are indicated by vertical dotted lines. For reference, the Fe 3d band of the clean surface is also shown with dashed lines.

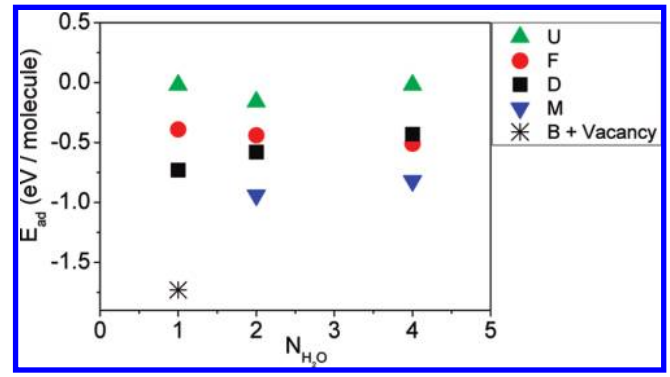

Figure 11. Adsorption energy (eV/molecule) obtained within GGA+*U* of different adsorbate systems as a function of the number of molecules per $(\sqrt{2} \times \sqrt{2})R45°$ unit cell.

The analysis of the bonding mechanism above suggests that GGA+*U* gives a more reliable description of the surface and adsorption properties of $Fe_3O_4(001)$.

3.6. Adsorption Energy as a Function of Coverage. To obtain a full picture of the water interaction with $Fe_3O_4(001)$, we discuss here the energetic trends as a function of water coverage. The adsorption energies for different coverages are plotted in Figure 11 and displayed also in Table 2. For an isolated molecule on a defect-free $Fe_3O_4(001)$ surface, we find that the most stable adsorbate configuration is a dissociated molecule (−0.76 eV) where the released hydrogen forms an OH group with a surface oxygen. This is followed by a molecular adsorption in a flat geometry (−0.39 eV) with the hydrogens pointing toward neighboring surface oxygens. On a

defective surface, we find a strong tendency toward dissociation (GGA+U, −1.73 eV), where the OH group occupies the oxygen vacancy and the proton is bound at a more distant surface oxygen site. The high adsorption energy indicates that, as soon as water is present in the atmosphere, it will adsorb and dissociate at defect sites, thus eliminating surface defects. This is consistent with the observation of Kendelewicz et al.[10] in the water pressure regime prior to extensive hydroxylation.

The adsorption of a second molecule results in an intermolecular bonding and a crossover to a partial dissociation (GGA+U, −0.94). In this case, the intact molecule forms a hydrogen bond to the neighboring OH group. A dissociative adsorption is 0.36 eV less favorable.

The mixed adsorption mode prevails also when a full saturation of the surface cation sites is reached after adsorption of four H_2O molecules. Here, the H_2O molecule is oriented with one hydrogen toward the next OH group and with the second pointing toward a surface oxygen, thus forming a 1D chain of alternating hydrogen-bonded flat water molecules and OH groups along the [110] direction. The two lone pairs of the water molecule play an important role by promoting the intermolecular hydrogen bonding, which can be comparable in strength to the water−substrate bonding.[2] A full dissociation is ∼0.40 eV less favorable.

A common feature to all dissociated or partially dissociated configurations is that the proton attaches to a surface oxygen without a tetrahedral iron neighbor. Protonation of O^S with an Fe_A neighbor is highly unfavorable. With increasing coverage, we observe that the binding energy for the dissociative adsorption decreases slightly, indicating a repulsive adsorbate−adsorbate interaction. In the case of molecular flat/titlted adsorption, the adsorption energy slightly increases with coverage due to hydrogen bond formation.

Because of the stronger interaction with the surface, water is bound more strongly on oxide surfaces compared with transition and noble metal surfaces. In the latter case, adsorption energies are typically in the range between −0.1 and −0.5 eV.[42,43] For oxide surfaces, the adsorption energy of a single water molecule ranges from −0.3 to −0.8 eV on Fe_2 $O_3(0001)$,[44] −0.57 eV on kaolinite,[45] −0.61 eV on NiO(001) (within GGA+U),[46] and −1.27 eV on zircon.[47] The adsorption energies for the mixed adsorption on $Fe_3O_4(001)$ (−0.8 to −0.9 eV) found in this study are similar to values reported for $TiO_2(110)$[38] (−1.0 eV). On $Fe_3O_4(111)$, an OH_3^+−OH overlayer was reported with an adsorption energy of −0.85 eV within GGA+U.[28]

4. Summary

In summary, we present a comprehensive DFT study of the initial adsorption of water on the $Fe_3O_4(001)$ surface, analyzing also the underlying electronic mechanisms. We find that electronic correlations (described here within GGA+U) affect notably the width and position of the Fe^{3+} 3d band and thereby influence the hybridization with the MO of the adsorbate and the resulting binding strength. Our results establish that, for isolated molecules, a heterolytic dissociation is most favorable, especially at surface defect sites. Although the surface octahedral Fe ions remain in a 3+ valence state, the protonation of surface oxygen results in an electron transfer to a subsurface Fe that becomes Fe^{2+}. On the nondefective surface, dissociation is followed in stability by a molecular adsorption where a flat/tilted molecule forms hydrogen bonds to surface oxygen. With increasing coverage, we obtain a crossover to a mixed adsorption where a hydrogen-bonded network forms between the alternating water molecules and OH groups. Such an adsorption mode has been reported for several other oxide surfaces, for example, rutile $TiO_2(110)$,[38] anatase $TiO_2(001)$,[39] MgO(001),[40] and $Al_2O_3(0001)$ surfaces.[41] The partial dissociation leads to different surface species, that is, water molecules and OH groups on top of Fe_BS as well as OH groups involving a surface oxygen. These different functional groups and the induced electron transfer processes may have important implications for the adsorption of further molecules and the catalytic activity of $Fe_3O_4(001)$.

Acknowledgment. We acknowledge discussions with W. Moritz, M.-L-Bocquet, funding by the DFG/PE883/1-2 and a grant for computational time at the HLRBII supercomputer at the Leibniz Rechenzentrum.

References and Notes

(1) Henderson, M. A. *Surf. Sci. Rep.* **2002**, *46*, 1.
(2) Thiel, P. A.; Madey, T. E. *Surf. Sci. Rep.* **1987**, *7*, 211.
(3) Ohe, K.; Tagai, Y.; Nakamura, S.; Oshima, T.; Baba, Y. *J. Chem. Eng. Jpn.* **2005**, *38*, 671.
(4) Katsumata, H.; Kaneco, S.; Inomata, K.; Itoh, K.; Funasaka, K.; Masuyama, K.; Suzuki, T.; Ohta, K. *J. Environ. Manage.* **2003**, *69*, 187.
(5) Martos, C.; Dufour, J.; Ruiz, A. *Int. J. Hydrogen Energy* **2009**, *34*, 4475.
(6) (a) Tasker, P. W. *J. Phys. C: Solid State Phys.* **1979**, *12*, 4977. (b) Tasker, P. W. *Philos. Mag. A* **1979**, *12*, 4977.
(7) Pentcheva, R.; Wendler, F.; Meyerheim, H. L.; Moritz, W.; Jedrecy, N.; Scheffler, M. *Phys. Rev. Lett.* **2005**, *94*, 126101.
(8) Lodziana, Z. *Phys. Rev. Lett.* **2007**, *99*, 206402.
(9) Reissner, R.; Schultze, M. *Surf. Sci.* **2001**, *482*, 285.
(10) Kendelewicz, T.; Liu, P.; Doyle, C. S.; Brown, G. E., Jr.; Nelson, E. J.; Chambers, S. A. *Surf. Sci.* **2000**, *453*, 32.
(11) Liu, P.; Kendelewicz, T.; Brown, G. E., Jr.; Nelson, E. J.; Chambers, S. A. *Surf. Sci.* **1998**, *417*, 53.
(12) Peden, C. H. F.; Herman, G. S.; Ismagilov, I. Z.; Kay, B. D.; Henderson, M. A.; Kim, Y.-J.; Chambers, S. A. *Catal. Today* **1999**, *51*, 513.
(13) Kundu, T. K.; Hanumantha Rao, K.; Parker, S. C. *J. Colloid Interface Sci.* **2006**, *295*, 364.
(14) Rustad, J. R. *Geochim. Cosmochim. Acta* **2002**, *67*, 1001.
(15) Mulakaluri, N.; Pentcheva, R.; Wieland, M.; Moritz, W.; Scheffler, M. *Phys. Rev. Lett.* **2009**, *103*, 176102.
(16) Reuter, K.; Scheffler, M. *Phys. Rev. B* **2001**, *65*, 035406.
(17) Blaha, P.; Schwarz, K.; Madsen, G. K. H.; Kvasnicka, D.; Luitz, J. *WIEN2k: An Augmented Plane Wave + Local Orbitals Program for Calculating Crystal Properties*; Karlheinz Schwarz, Technische Universität Wien: Wien, Austria, 2001; ISBN 3-9501031-1-2.
(18) Perdew, J. P.; Burke, K.; Ernzerhof, M. *Phys. Rev. Lett.* **1996**, *77*, 3865.
(19) Anisimov, V. I.; Solovyev, I. V.; Korotin, M. A.; Czyzyk, M. T.; Sawatzky, G. A. *Phys. Rev. B* **1993**, *48*, 16929.
(20) Leonov, I.; Yaresko, A. N.; Antonov, V. N.; Korotin, M. A.; Anisimov, V. I. *Phys. Rev. Lett.* **2004**, *93*, 146404.
(21) Jeng, H.-T.; Guo, G. Y.; Huang, D. J. *Phys. Rev. Lett.* **2004**, *93*, 156403.
(22) Kurth, S.; Perdew, J. P.; Blaha, P. *Int. J. Quantum Chem.* **1999**, *75*, 889.
(23) While the atomization energies of most molecules are well described within GGA, a larger error is observed for O_2.[22] However, here, we are interested in energy differences between various adsorbate configurations, where the uncertainty in the description of these reference energies cancels out. Moreover, the energy of the oxygen molecule is used only for calculating the formation energy of oxygen vacancies on the defective $Fe_3O_4(001)$ surface.
(24) (a) Kresse, G.; Furthmüller, J. *Phys. Rev. B* **1996**, *54*, 11169. (b) Kresse, G.; Furthmüller, J. *Comput. Mater. Sci.* **1996**, *6*, 15. (c) Kresse, G.; Joubert, D. *Phys. Rev. B* **1999**, *59*, 1758.
(25) Pentcheva, R.; Moritz, W.; Rundgren, J.; Frank, S.; Schrupp, D.; Scheffler, M. *Surf. Sci.* **2008**, *602*, 1299.
(26) Fonin, M.; Pentcheva, R.; Dedkov, Yu., S.; Sperrlich, M.; Vyalikh, D. V.; Scheffler, M.; Rüdiger, U.; Güntherodt, G. *Phys. Rev. B* **2005**, *72*, 104436.
(27) We have also performed calculations for a hydroxylated 0.5 A-layer termination; however, it remained energetically unfavorable compared with systems containing a B layer.
(28) Grillo, M. E.; Finnis, M. W.; Ranke, W. *Phys. Rev. B* **2008**, *77*, 075407.
(29) Lang, N. D. *Solid State Commun.* **1971**, *9*, 1015.
(30) Muscat, J. E.; Newns, D. M. *Surf. Sci.* **1978**, *74*, 355.

(31) Carrasco, J.; Michaelides, A.; Scheffler, M. *J. Chem. Phys.* **2009**, *130*, 184707.
(32) Nillson, A.; Pettersson, L. J. M.; Norksov, J. K. *Chemical Bonding at Surface and Interfaces*; Elsevier: Amsterdam, 2008.
(33) Scheffler, M.; Stampfl, C. Theory of Adsorption on Metal Substrates. In *Handbook of Surface Science*, Vol. 2, Electronic Structure; Horn, K., Scheffler, M., Eds.; Elsevier: Amsterdam, 2000.
(34) Santra, B.; Michaelides, A.; Scheffler, M. *J. Chem. Phys.* **2007**, *127*, 184104.
(35) Santra, B.; Michaelides, A.; Fuchs, M.; Tkatchenko, A.; Filippi, C.; Scheffler, M. *J. Chem. Phys.* **2008**, *129*, 194111.
(36) Morgan, B. J.; Watson, G. W. *Surf. Sci.* **2007**, *601*, 5034.
(37) Jordan, K.; Cazacu, A.; Manai, G.; Ceballos, S. F.; Murphy, S.; Shvets, I. V. *Phys. Rev. B* **2006**, *74*, 085416.
(38) Lindan, P. J. D.; Harrison, N. M.; Gillan, M. J. *Phys. Rev. Lett.* **1998**, *80*, 762.
(39) Vittadini, A.; Selloni, A.; Rotzinger, F. P.; Gratzel, M. *Phys. Rev. Lett.* **1998**, *81*, 2954.
(40) Odelius, M. *Phys. Rev. Lett.* **1999**, *82*, 3919.
(41) Thissen, P.; Grundmeier, G.; Wippermann, S.; Schmidt, W. G. *Phys. Rev. B* **2009**, *80*, 245403.
(42) Michaelides, A.; Ranea, V. A.; de Andres, P. L.; King, D. A. *Phys. Rev. Lett.* **2003**, *90*, 216102.
(43) Ren, J.; Meng, S. *Phys. Rev. B* **2008**, *77*, 054110.
(44) Yin, S.; Ma, X.; Ellis, D. E. *Surf. Sci.* **2007**, *601*, 2426.
(45) Hu, X. L.; Michaelides, A. *Surf. Sci.* **2008**, *602*, 960.
(46) Yu, N.; Zhang, W.-B.; Wang, N.; Wang, Y.-F.; Tang, B.-Y. *J. Phys. Chem. C* **2008**, *112*, 452.
(47) Balan, E.; Mauri, F.; Muller, F.; Calasi, G. *Am. Mineral.* **2001**, *86*, 910.

JP100344N